Biointerface Research in Applied Chemistry
Open-Access Journal (ISSN: 2069-5837)

Article
Volume 13, Issue 4, 2023, 394
https://doi.org/10.33263/BRIAC134.394

Double Diffusion, Chemical Reaction, and Heat Source Effects on Magnetohydrodynamic Flow of Copper and Silver Water-based Nanofluids over a Moving Vertical Porous Plate

Santha Raju Medepalli [1,*], Sankara Sekara Raju Gurrammagari [2]

[1] Department of Mathematics, JNT University Anantapur, Ananthapuramu, Andhra Pradesh, India; santharajusrkgac@gmail.com (S.R.M.);
[2] Department of Mathematics, JNTUA College of Engineering, Pulivendula, Andhra Pradesh, India; rajugss@yahoo.com (S.S.R.G.);
* Correspondence: santharajusrkgac@gmail.com (S.S.R.G.);

Received: 15.06.2022; Accepted: 30.07.2022; Published: 1.11.2022

Abstract: In this manuscript, the impact of Soret and Dufour numbers on magnetohydrodynamic (MHD) flow for Silver (Ag) and Copper (Cu) water-based nanofluids past a moving plate over a porous medium are investigated numerically. The influences of heat sources and chemical reactions are also considered, as their applications are prevalent in several industries. The flow's constituents' governing equations are coupled with Partial differential equations (PDEs) that are converted into a dimensionless form using appropriate flow parameters. Subsequently, the finite-difference technique is used to resolve the resulting equations. The varied effects of flow parameters on the momentum, temperature, and concentration boundary layers are investigated using various graphs. The results presented in terms of non-dimensional parameters like shear stress factor, Sherwood number, and Nusselt number of fluids are tabulated for the nanofluids Ag-water and Cu-water. It is found that the augmented values of Dufour and Soret numbers enhance the fluid velocity. However, the species concentration decreases in the existence of Dufour and chemical reaction effects.

Keywords: nanofluid; magnetohydrodynamic; Soret effect; porous medium; Dufour effect; finite-difference method.

Nomenclature:

B_0	Applied magnetic field (NmA^{-1})
$\bar{C}$	Species concentration (Kgm^{-3})
$\bar{C}_w$	Constant concentration (Kgm^{-3})
$\bar{C}_\infty$	Concentration of the fluid in a free stream (Kgm^{-3})
C_P	Specific heat at constant pressure ($Jkg^{-1}K$)
Du	Dufour number
D	Mass-diffusion coefficient (m^2s^{-1})
D_1	Thermal-diffusion coefficient (m^2s^{-1})
Gr	Thermal-Grashof number
Gc	Mass-Grashof number
g	Acceleration due to gravity (ms^{-2})
k	Thermal conductivity ($Wm^{-1}K^{-1}$)
K	Permeability parameter
K^*	Permeability of the porous medium (m^2)
k_1	Absorption coefficient (m^{-1})

Kr	Dimensionless chemical reaction parameter
K_r^1	Chemical reaction parameter
M	Magnetic parameter
Nr	Radiation parameter
Nu	Nusselt number
Pr	Prandtl number
Q_0	Heat source
q_r^*	Radiative heat flux (Wm^{-2})
Q	Dimensionless heat source
So	Soret number
Sh	Sherwood number
Sc	Schmidt number
t	Dimensionless time
$\overline{t}$	Time (s)
$\overline{T}$	Temperature (K)
$\overline{T}_\infty$	Temperature of the fluid in a free stream (K)
$\overline{T}_w$	Constant temperature (K)
$\overline{u}$	Velocity of the fluid along $\overline{x}$ -direction (ms^{-1})
v_f	Kinematic viscosity (m^2s^{-1})
$\overline{y}$	Coordinate perpendicular to the plate (m)
Greek Symbols	
β	Thermal expansion coefficient (K^{-1})
β^*	Mass transfer coefficient
η	Dimensionless coordinate
Θ	Dimensionless temperature
λ	Direction of motion of a plate
μ	Dynamic viscosity ($Kgm^{-1}s^{-1}$)
ρ	Density (Kgm^{-3})
σ	Electrical conductivity (Sm^{-1})
σ^*	Stefan-Boltzman constant ($Wm^{-2}K^{-4}$)
τ	Skin friction coefficient
Φ	Dimensionless velocity
φ	Volume fraction of nanoparticle
Ψ	Dimensionless concentration
Subscripts	
s	Solid-phase
nf	Nanofluid
f	Fluid phase

1. Introduction

Nowadays, nanotechnology is speedily impacting researchers and scientists due to its simplicity and wide applications in various fields of the modern sciences. For example, in the drug field, nanofluids-based administrators deal with malignant growth patients, involving different radiations and meds. On the other hand, the cooling and heating process is more important in our daily lives, like reducing the heat of nuclear reactors, hotness from computer central processing units, cooling down the radiators in automobiles, and treating warm streams in heat valves nano-liquids. Nanofluids submerged in normal liquids tend to improve their thermal properties of liquids. Chai [1] first introduced nanofluids by combining nano-sized particles in base fluids. Carbon nanotubes, carbides, and metals can be used to form particles. Nanofluids have numerous mechanical applications: for example, nuclear reactors, heat exchangers, space vehicles, water heating solar, chillers, refrigerator-freezers, guards of lighter-weight vehicles, lubricants, and heat sinks of micro-channel. Veera Krishna *et al.* [2] examined the influences of radiation absorption and magnetic field on unsteady MHD nanofluid flow over a traveling plate. Dharmaiah *et al.* [3] discussed the effects of diffusion thermo, radiation-absorption, and Hall and ion slip on MHD nanofluid flow past the permeable

moving plate. Khan *et al*. [4] deliberate the effect of mass and heat transfer in a Maxwell and molybdenum disulfide-engine oil nanofluid flow over a plate with isothermal and ramped wall concentration and temperature. Ahmed *et al*. [5] exponentially discussed the influence of activation energy and variable thermal conductivity on MHD Williamson nanofluid over a curved stretching surface. Sravanthi *et al*. [6] numerically examined the effect of moving plates on magnetite-water nanofluid. Because of its significance, numerous researchers (Baby Rani *et al*. [7]; Srinivasulu *et al*. [8]; Noranuar *et al*. [9]; Sarkar *et al*. [10]; and Swain *et al*. [11]; and Sharma *et al.* [12]) have examined nanofluid flow at various velocities and in various designs.

The relevance and diverse uses of free convective flow and heat transmission have recently sparked a resurgence of investigation and study in extrusion, mechanical forming processes, food processing, glass-fiber production processes, melt spinning, and other processes. Researchers have increasingly focused on thermal and mass transfer in MHD flow due to the vast range of applications in engineering and industry. Just a few examples include magnetic material processing, geophysics, and cooling rate control. Veera Krishna *et al*. [13] conferred the ion slip and hall effects on convective rotating MHD second-grade fluid flow over a moving and permeable vertical surface. Prabhakar Reddy and Sademaki [14] presented the oscillating porous plate influence on MHD Casson fluid flow with Newtonian Heating. Nabwey *et al*. [15] Reported and studied the mixed convection nanofluid flow of Gyrotactics microorganisms past a permeable plate with velocity slip and variable viscosity. Arulmozhi *et al*. [16] deliberated the chemical reactive and radiative impacts on MHD nanofluid flow over a moving plate.

Thermal radiation is a critical concern in a range of industrial operations, including electrical power generation, glass manufacturing, solar power technologies, and furnace design. Rooman *et al*. [17] examined the effect of thermal radiation on MHD Williamson nanofluid flow over a Riga vertical plate. Krishna *et al*. [18] scrutinized the influence of thermal radiation on MHD Casson hybrid nanofluid flow over the plate accelerated exponentially. Wahid *et al*. [19] presented the impact of thermal radiation on MHD hybrid nanofluid convective flow over a flat plate. Kumar *et al*. [20] studied the impact of thermal radiation on MHD convective nanofluid flow over a plate. The effect of Thermal radiation on squeezing MHD unsteady nanofluid flow between plates is investigated by Ullah *et al*. [21].

Chemical reaction expertise is applied in a wide range of engineering and technological fields, including the chemical industry, polymer processing, food processing, and the glass manufacturing sector, to name a few. Rahman and Uddin [22] illustrated the impact of variable chemical reactions on MHD radiative nanofluid flow through an endless upright vertical plate. Goud Bejawada *et al*. [23] deliberated the impact of chemical reactions on MHD Casson fluid flow embedded in an inclined surface with a Forchheimer porous medium. An investigation of Prandtl MHD nanofluid flow of convective boundary conditions passed through a stretched sheet with chemical reaction, and thermal radiation was studied by Patil *et al.* [24]. Cui *et al*. [25] scrutinized the effect of chemical reactions on the stagnation flow of nanofluid on a solid plate along with motile microorganisms.

Researchers have devoted the past four decades to the double-diffusive phenomena because of their various applications in solid-state physics, chemical engineering, geophysics, oceanography, production of pure medication, liquid gas storage, high-quality crystal production, and oceanography, solidification of molten alloys, magmas, and geothermally heated lakes. The thermal-diffusion (Soret) effect is the name given to the mass flux produced

by a temperature gradient. The diffusion-thermo (Dufour) effect is the name given to the energy flux brought on by concentration changes. Mondal *et al*. [26] examined the Double-diffusion and thermophoresis effects on MHD convective fluid flow along with an infinite permeable inclined plate. Oyekunle *et al*. [27] conferred the effect of double diffusion on MHD slip flow over a permeable plate. Ahammad *et al*. [28] conveyed the effect of Double diffusion on unsteady boundary layer flow over the vertical channel with suction and viscous dissipation. Siddique *et al*. [29] presented the influence of diffusion-thermo and thermal-diffusion effects on second-grade MHD nanofluid flow over a stretching surface.

Heat generation/absorption is another important component in fluid flow. Processes such as heat treatment, ventilation, and air conditioning have important applications in the food business, thermal engineering, mechanical engineering, and physics. Ganga *et al*. [30] presented the influence of internal heat generation/absorption on MHD radiative fluid flow across a vertical plate. Anwar *et al*. [31] explored the Titanium oxide (TiO2) and Copper (Cu) nanoparticles analytically through porous vertical plates by considering the heat sink/source and radiative effects. Dharmaiah *et al*. [32] studied the impact of heat source, thermophoresis, and hall current on MHD dissipative convective fluid flow about the inclined plate analytically. Mishra *et al*. [33] conferred the influence of heat generation/absorption and Joule heating on MHD nanofluid flow past a permeable stretching/shrinking channel. Patel *et al*. [34] scrutinized the influences of heat generation and cross-diffusion on MHD Carreau fluid flow towards an infinite plate.

In all the above investigations, researchers focused on studying the radiation effects through the porous media. It is found that, in the presence of Soret, Dufour, and heat source along with chemical reaction effects were not addressed by them. Hence, further studies are required to extend the work on the impacts of Soret, heat source, and Dufour on the MHD radiating nanofluid flow across a vertical porous plate. Pure water (H_2O) is used as a base liquid in this investigation and contains two types of nanoparticles: Ag and Cu. Taylor series expansion converts the nonlinear term in the governing equations into a linear term.

2. Mathematical Model

It considers the flow of one-dimensional magnetohydrodynamic and radiating nanofluid through an infinite plate immersed in a porous material seen in Figure 1. It is assumed that Soret, Dufour, chemical reaction, and heat source effects exist. Figure 1 shows the flow direction along the $\bar{y}$ -axis and the vertical plate along the $\bar{x}$ -axis. B0 is parallel to the $\bar{y}$ -axis and perpendicular to the $\bar{x}$ -axis. The plate is stationary with concentration, $\bar{C}_\infty$ and temperature, $\bar{T}_\infty$ at $\bar{t} = 0$. When $\bar{t} > 0$, the vertical plate starts moving with velocity λu_0 in its plane, u_0 is constant, the species concentration is maintained at $\bar{C}_w$ and the plate's hotness is raised or reduced to $\bar{T}_w$. The pressure gradient caused by the magnetic field and other external factors, such as fluid polarization, is neglected. The magnetic Reynolds number of metallic liquids and ionized fluids is small. When compared to the imposed magnetic field, the flow's magnetic field is insignificant. q_r^* is applied normally to the plate; however, it is insignificant in the $\bar{x}$ -direction. It is proposed to consider water-based nanofluids with Cu and Ag nanoparticles, and the corresponding thermal and physical properties are presented in Table 1. Moreover, an assumption of thermal equilibrium between water and nanoparticles is made.

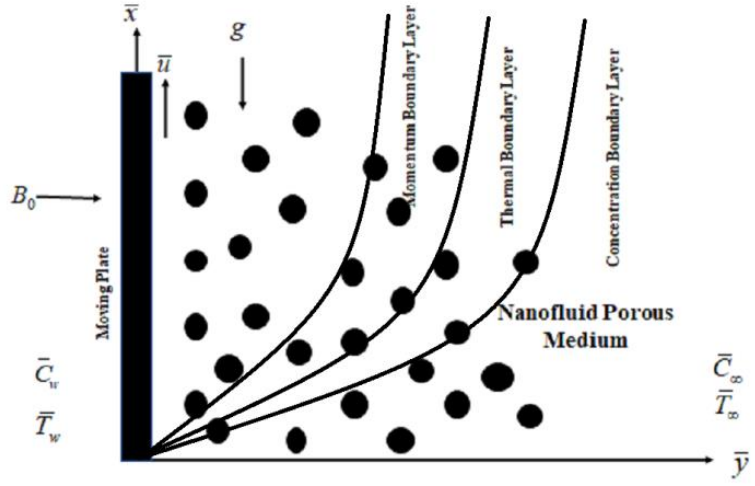

Figure 1. The geometry of the flow problem.

Table 1. Thermo-physical properties of H_2O, Ag, and Cu (Anwar *et al.* [31]; Mishra *et al.* [35]).

Physical properties	H_2O	Ag	Cu
ρ (Kg/m^3)	997.1	10500	8933
σ (sm^{-1})	5.5x10^{-6}	6.3x10^7	59.6x10^6
β x10^5 (K^{-1})	21	1.89	1.67
C_p (J/Kg K)	4179	235	385
k (W/mK)	0.613	429	401

The momentum, energy, and species concentration equations are as follows, based on the above assumptions and Anwar *et al.* [31], Chandra Reddy *et al.* [36], Dharmaiah *et al.* [3]

$$\rho_{nf}\left[\frac{\partial \bar{u}}{\partial \bar{t}}\right]=\mu_{nf}\left[\frac{\partial^2 \bar{u}}{\partial \bar{y}^2}-\frac{\bar{u}}{K^*}\right]-\sigma_{nf}B_0^2\bar{u}+g\left(\rho\beta^*\right)_{nf}\left(\bar{C}-\bar{C}_\infty\right)+g\left(\rho\beta\right)_{nf}\left(\bar{T}-\bar{T}_\infty\right) \quad (1)$$

$$\frac{\partial \bar{T}}{\partial \bar{t}}=\frac{\mathrm{K}_{nf}}{\left(\rho C_p\right)_{nf}}\frac{\partial^2 \bar{T}}{\partial \bar{y}^2}+\frac{Q_0}{\left(\rho C_p\right)_{nf}}\left(\bar{T}-\bar{T}_\infty\right)-\frac{1}{\left(\rho C_p\right)_{nf}}\frac{\partial q_r^*}{\partial \bar{y}}+\frac{D_M K_T}{\left(\rho C_p\right)_{nf} C_S}\frac{\partial^2 \bar{C}}{\partial \bar{y}^2} \quad (2)$$

$$\frac{\partial \bar{C}}{\partial \bar{t}}=D\frac{\partial^2 \bar{C}}{\partial \bar{y}^2}+D_1\frac{\partial^2 \bar{T}}{\partial \bar{y}^2}-K_r^1(\bar{C}-\bar{C}_\infty) \quad (3)$$

where

$$\rho_{nf}=\rho_f-\varphi\left[\rho_f-\rho_s\right],\ \mu_{nf}=\frac{\mu_f}{\left[1-\varphi\right]^{2.5}},\ \sigma_{nf}=\left[1+\frac{3\varphi(\sigma-1)}{(\sigma+2)-(\sigma-1)\varphi}\right]\sigma_f,\ \left(\rho\beta\right)_{nf}=\left(\rho\beta\right)_f-\varphi\left[\left(\rho\beta\right)_f-\left(\rho\beta\right)_s\right],$$

$$\left(\rho C_P\right)_{nf}=\left(\rho C_P\right)_f-\varphi\left[\left(\rho C_P\right)_f-\left(\rho C_P\right)_s\right],\ \left(\rho\beta^*\right)_{nf}=\varphi\left(\rho\beta^*\right)_s+\left[1-\varphi\right]\left(\rho\beta^*\right)_f,\ \sigma=\frac{\sigma_s}{\sigma_f}.$$

Eqs. (1) - (3) are only applicable to spherical nanoparticles and do not consider the different states of nanoparticles. The effective thermal conductivity of the nanofluid delineated by Tlili *et al.* [37] and Kakac and Pramuanjaroenkij [38] is provided by the following equation:

$$k_{nf}=\left(\left[\frac{\left(k_s+2k_f-2\left(k_f\varphi-k_s\varphi\right)\right)}{k_s+2k_f+k_f\varphi-k_s\varphi}\right]k_f\right) \quad (4)$$

The initial & boundary conditions are

$$\begin{aligned}&\bar{u}(\bar{y},0)=0,\ \bar{T}(\bar{y},0)=\bar{T}_\infty,\ \bar{C}(\bar{y},0)=\bar{C}_\infty,\ \forall\ \bar{y}\geq 0\\&\bar{u}(\bar{y},\bar{t})\to 0,\ \bar{T}(\bar{y},\bar{t})\to\bar{T}_\infty,\ \bar{C}(\bar{y},\bar{t})\to\bar{C}_\infty,\ \text{as}\ \bar{y}\to\infty,\bar{t}>0\\&\bar{u}(0,\bar{t})=\lambda u_0,\ \bar{T}(0,\bar{t})=\bar{T}_w,\ \bar{C}(0,\bar{t})=\bar{C}_w,\ \forall\ \bar{t}>0\end{aligned}\tag{5}$$

where, λ is the direction of the plate's motion, with λ =0 for the fixed plate and $\lambda=\pm1$ for the forward and backward motion.

Under the Rosseland approximation, q_r^* is of the form,

$$q_r^*=-\left[\frac{4\sigma^*}{3k_1}\left(\frac{\partial\bar{T}^4}{\partial\bar{y}}\right)\right]\tag{6}$$

The Taylor series expansion of $\bar{T}^4$ about $\bar{T}_\infty$ is $\bar{T}^4=\bar{T}_\infty^4+4\left[\bar{T}-\bar{T}_\infty\right]\bar{T}_\infty^3+6\left[\bar{T}-\bar{T}_\infty\right]^2\bar{T}_\infty^2+\ldots.$

Assuming that the temperature distinction inside the liquid is low, ignoring higher-order terms in the above expression. On further simplification,

$$\bar{T}^4=4\bar{T}_\infty^3\bar{T}-3\bar{T}_\infty^4\tag{7}$$

On substitution of Eqs. (6), and (7) in Eq. (2), we get,

$$\left(\rho C_p\right)_{nf}\frac{\partial\bar{T}}{\partial\bar{t}}=\left(k_{nf}+\frac{16\sigma^*\bar{T}_\infty^3}{3k_1}\right)\frac{\partial^2\bar{T}}{\partial\bar{y}^2}+Q_o(\bar{T}-\bar{T}_\infty)+\frac{D_M K_T}{C_S}\frac{\partial^2\bar{C}}{\partial\bar{y}^2}\tag{8}$$

Define,

$$\Phi=\frac{\bar{u}}{u_0},t=\frac{u_0^2\bar{t}}{v_f},\eta=\frac{u_0\bar{y}}{v_f},\Psi=\frac{\bar{C}-\bar{C}_\infty}{\bar{C}_w-\bar{C}_\infty},\Theta=\frac{\bar{T}-\bar{T}_\infty}{\bar{T}_w-\bar{T}_\infty}\tag{9}$$

From Eq. (9), the Eqs. (1), (3), and (8) become

$$\frac{\partial\Phi}{\partial t}=a_1\frac{\partial^2\Phi}{\partial\eta^2}-M^2a_4\Phi-\frac{a_1}{K}\Phi+Gra_2\Theta+Gca_3\Psi\tag{10}$$

$$\frac{\partial\Theta}{\partial t}=a_5\frac{\partial^2\Theta}{\partial\eta^2}+a_6\Theta+a_7\frac{\partial^2\Psi}{\partial\eta^2}\tag{11}$$

$$\frac{\partial\Psi}{\partial t}=\frac{1}{Sc}\frac{\partial^2\Psi}{\partial\eta^2}-Kr\Psi+So\frac{\partial^2\Psi}{\partial\eta^2}\tag{12}$$

where,

$$a_1=\frac{1}{(1-\varphi)^{2.5}x_1},a_2=\left[\frac{x_2}{x_1}\right],a_3=\left[\frac{x_3}{x_1}\right],a_4=\left[\frac{x_4}{x_1}\right],a_5=\frac{1}{x_5\,\mathrm{Pr}}\left(x_6+Nr\right),a_6=\frac{Q}{x_5\,\mathrm{Pr}},a_7=\frac{Du}{x_5\,\mathrm{Pr}},$$

$$x_1=\varphi\left[\frac{\rho_s}{\rho_f}\right]-\varphi+1,x_2=\varphi\left[\frac{(\rho\beta)_s}{(\rho\beta)_f}\right]-\varphi+1,\ x_3=\varphi\left[\frac{\left(\rho\beta^*\right)_s}{\left(\rho\beta^*\right)_f}\right]-\varphi+1,x_4=\frac{3(\sigma-1)\varphi}{(\sigma+2)-(\sigma-1)\varphi}+1,\sigma=\frac{\sigma_s}{\sigma_f},$$

$$x_5=\varphi\left[\frac{\left(\rho c_p\right)_s}{\left(\rho c_p\right)_f}\right]-\varphi+1,x_6=\frac{k_s-2\varphi\left(k_f-k_s\right)+2k_f}{k_s+\varphi\left(k_f-k_s\right)+2k_f},\ Gr=\frac{v_f g\beta_f\left(\bar{T}_w-\bar{T}_\infty\right)}{u_0^3},Gc=\frac{v_f g\beta_f^*\left(\bar{C}_w-\bar{C}_\infty\right)}{u_0^3},M^2=\frac{v_f B_0^2\sigma_f}{\rho_f u_o^2},$$

$$K=\frac{u_0^2k^*}{v_f^2},\mathrm{Pr}=\frac{\mu_f\left(c_p\right)_f}{k_f},Nr=\frac{16\sigma^*\bar{T}_\infty^3}{3k_1k_f},Q=\frac{Q_0v_f^2}{k_fu_o^2},Sc=\frac{v_f}{D},Kr=\frac{k_r^1v_f}{u_o^2},So=\frac{D_1\left(\bar{T}_w-\bar{T}_\infty\right)}{v_f\left(\bar{C}_w-\bar{C}_\infty\right)},Du=\frac{D_MK_T}{k_fC_S}\frac{\bar{C}_w-\bar{C}_\infty}{\bar{T}_w-\bar{T}_\infty}$$

Initial & boundary conditions Eq. (5) becomes

$$\begin{aligned}&\Phi(\eta,0)=0,\ \Theta(\eta,0)=0,\ \Psi(\eta,0)=0\ \forall\ \eta\geq 0\\&\Phi(\eta,t)\to 0,\ \Theta(\eta,t)\to 0,\ \Psi(\eta,t)\to 0\ \text{as}\ t>0,\eta\to\infty\\&\Phi(0,t)=\lambda,\ \Theta(0,t)=1,\ \Psi(0,t)=1\ \forall\ t>0\end{aligned}\tag{13}$$

3. Solution of the Problem

Partial differential equations can be numerically solved using the finite difference method (FDM). It has been applied to a variety of problems. These include time-independent and dependent, linear, and nonlinear problems. Therefore, System of Eqs. (10) - (12) are one-dimensional linear, second-order, and coupled PDEs. These equations can be solved together by incorporating conditions seen in Eq. (13). The exact solutions for the system of equations are complicated to solve analytically due to their complexity in nature. Therefore, other alternative methods have to be chosen. To solve the equations described above, the finite-difference technique was utilized. The finite difference of the system of equations is as follows.

$$\Phi(p,n_{13}) = a_{11}\left[\Phi(p,q)\right] + r_1\left[\Phi(n_{11},q) + \Phi(n_{12},q)\right] + a_{12}\left[\Theta(p,q)\right] + a_{13}\left[\Psi(p,q)\right] \quad (14)$$

$$\Theta(p,n_{13}) = b_{11}\left[\Theta(p,q)\right] + r_6\left[\Theta(n_{11},q) + \Theta(n_{12},q)\right] + r_{11}\left[\Psi(n_{11},q) - 2\Psi(p,q) + \Psi(n_{12},q)\right] \quad (15)$$

$$\Psi(p,n_{13}) = c_{11}\left[\Psi(p,q)\right] + r_8\left[\Psi(n_{11},q) + \Psi(n_{12},q)\right] + r_9\left[\Theta(n_{11},q) - 2\Theta(p,q) + \Theta(n_{12},q)\right] \quad (16)$$

where,

$$r_1 = \frac{r_5}{(\Delta\eta)^2},\ r_2 = a_2\Delta t,\ r_3 = a_3\Delta t,\ r_4 = a_4\Delta t,\ r_5 = a_1\Delta t,\ r_6 = \frac{a_5\Delta t}{(\Delta\eta)^2},\ r_7 = a_6\Delta t,\ r_8 = \frac{\Delta t}{Sc(\Delta\eta)^2},$$

$$r_9 = \frac{So\Delta t}{(\Delta\eta)^2},\ r_{10} = Kr\Delta t,\ r_{11} = \frac{a_7\Delta t}{(\Delta\eta)^2},\ a_{11} = 1 - 2r_1 - M^2 r_4 - \frac{r_5}{K},\ a_{12} = r_2 Gr,\ a_{13} = r_3 Gc,$$

$$b_{11} = 1 - 2r_6 + r_7,\ c_{11} = 1 - 2r_8 - r_{10},\ n_{11} = p - 1,\ n_{12} = p + 1,\ n_{13} = q + 1.$$

where, p denotes η, and q as t. In this method, the values at discrete points in the domain are grid points. The spacing of the grid points is uniform along the y-axis, is $\Delta\eta = 0.1$ and $\Delta t = 0.001$. On substituting the values of the grid points, Eq. (13) becomes

$$\Phi(p,0) = 0,\ \Theta(p,0) = 0,\ \Psi(p,0) = 0\ \ \forall\ p \quad (17)$$

and by incorporating boundary values of the grid points, Eq. (13) becomes

$$\Phi(p_m,q) = 0,\ \Theta(p_m,q) = 0,\ \Psi(p_m,q) = 0,\ \forall\ \mathrm{q} \quad (18)$$
$$\Phi(0,q) = \lambda,\ \Theta(0,q) = 1,\ \Psi(0,q) = 1,\ \forall\ \mathrm{q}$$

where, p_m=200.

The boundary conditions are shown in Eqs. (17) & (18) are used to compute the velocity $\Phi(p,q+1),\ p = 1,\ 200$ at each time step from Eq. (14). Moreover, it is followed by computing the temperature $\Theta(p,q+1)$ from Eq. (15) and concentration $\Psi(p,q+1)$ from Eq. (16). The cycle repeats until the time step $t = 0.5$.

3.1. Sherwood number, Nusselt number, and Skin friction coefficient.

The dimensionless numbers used in the current study are Sherwood (*Sh*), Nusselt (*Nu*), and skin friction or shear stress coefficient (τ), given by

$$Sh = -\left(\frac{\partial\Psi}{\partial\eta}\right)_{\eta=0},\ Nu = -\left(\frac{\partial\Theta}{\partial\eta}\right)_{\eta=0},\ \text{and}\ \tau = -\left(\frac{\partial\Phi}{\partial\eta}\right)_{\eta=0}$$

4. Results and Discussion

The obtained outcomes in terms of velocity Φ, temperature Θ, and concentration Ψ are discussed in Figures 3 - 18. Similarly, τ, *Nu*, and *Sh* are displayed in Tables 2 - 3. In the present analysis, we fixed the following parameter values in the numerical calculation as: *Gr* = 5.0, *Pr* = 6.8, *Q* = 0.5, M^2 = 10.0, *Nr* = 1.5, *K* = 5.0, *Kr* = 3.0, *Sc* = 0.22, *So* = 1.0, *Gc* = 5.0, *Du* = 0.1, φ = 0.1.

To ensure the exactness of the current technique, we compared our current results with the computational results of Chandra Reddy *et al*. [36], which consider the radiation *Nr* on Θ while ignoring the parameters Du, Q, Kr, and K. Figure 2 shows that it is in well-established agreement.

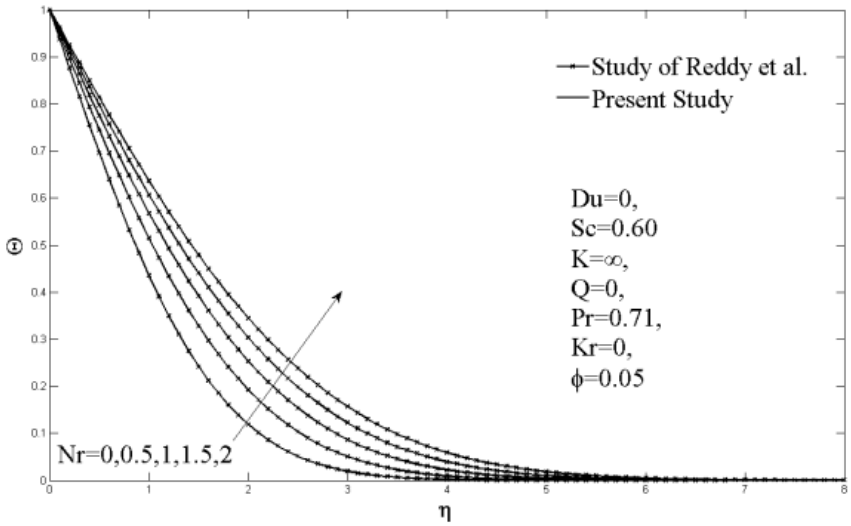

Figure 2. Comparing the influence of *Nr* on Θ with the study of Reddy *et al*. [36].

Figure 3 shows the velocity reports of nanofluids, Ag-water, and Cu-water. While comparing Ag-water to Cu-water, the Ag-water velocity has a thinner boundary layer for both stationary and moving plates. This is caused due to an upturn in its dynamic viscosity and comparatively greater density of nanoparticle Ag (Table 1). A comparison of two nanofluids for Θ and Ψ can be portrayed in Figure 4 & Figure 5, respectively. The temperature profile in Ag-water is higher than that of Cu-water, indicating that the thermal boundary layer in nanofluid Ag-water is growing. The reverse pattern is identified in the concentration profile, as shown in Figure 5.

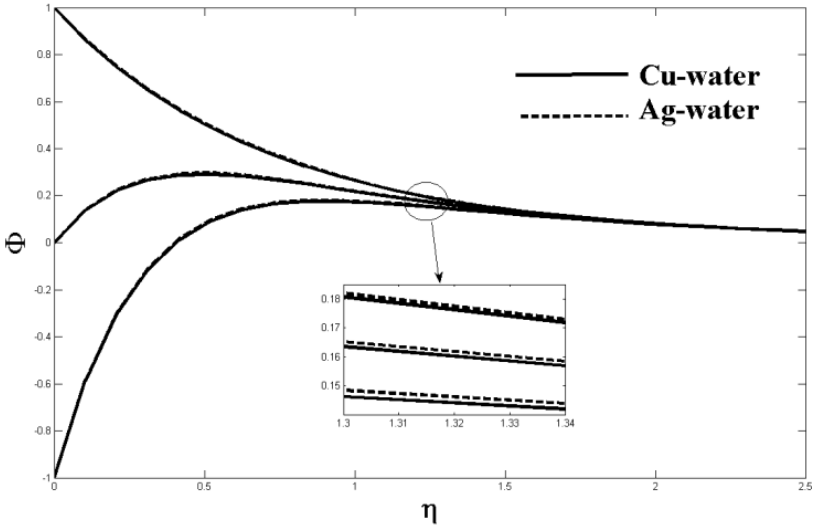

Figure 3. Comparison of nanofluids on Φ.

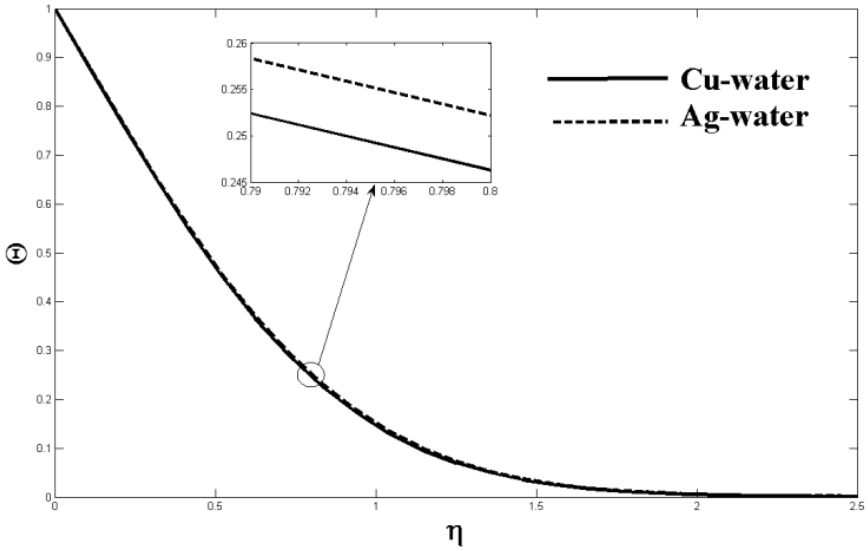

Figure 4. Comparison of nanofluids on Θ.

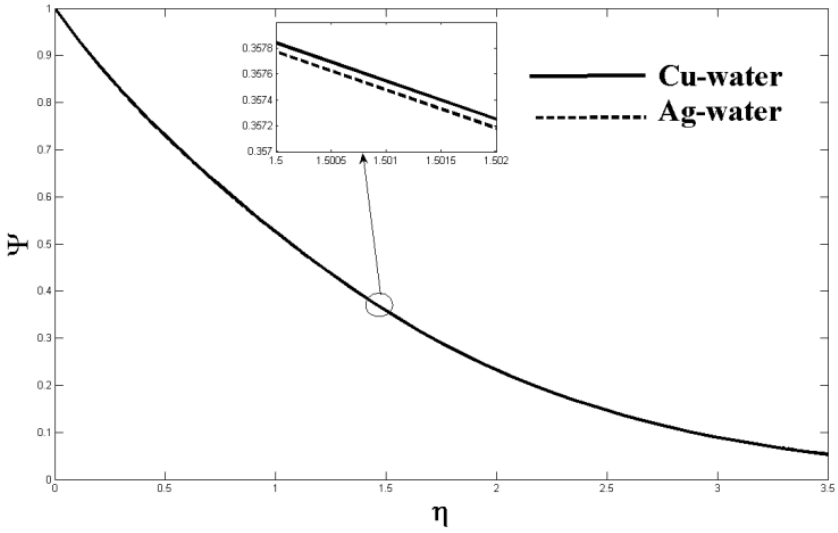

Figure 5. Comparison of nanofluids on Ψ.

Figures 6-8 show the impact of *Du* on the fluid's velocity, hotness, and species concentration distribution, respectively. The greater the *Du* value, the better the fluid velocity and temperature, but the species concentration of the nanofluids decreases. Figure 9 portrays the influence of *Gc* on Φ for both the nanofluids. Nanofluid velocity is increasing for various values of Gc for both stationary and moving plates. This is owing to the existence of thermal and solutal buoyancy, which causes the velocity to rise for both nanofluids. The impact of Kr on velocity and species concentration for both nanofluids is shown in Figures 10 & 11. For both stationary and moving plates, increased *Kr* values suppress nanofluid velocity and concentration. This is usually caused by an increase in interfacial mass transfer. Figures 12-14 exhibited the influence of φ on Φ, Θ and Ψ for both nanofluids, respectively. It was discovered that increased φ values resulted in a temperature rise but a reduction in fluid velocity. It can be observed that mixed performance in increasing/decreasing concentration profile.

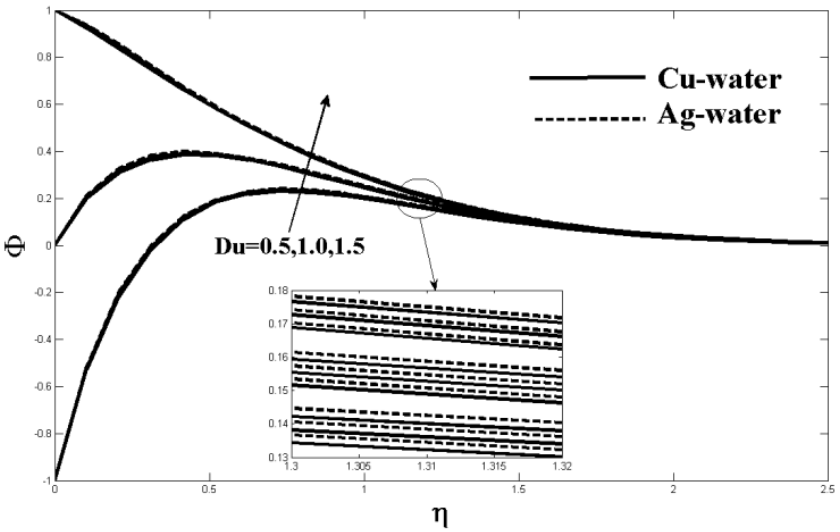

Figure 6. Du on Φ.

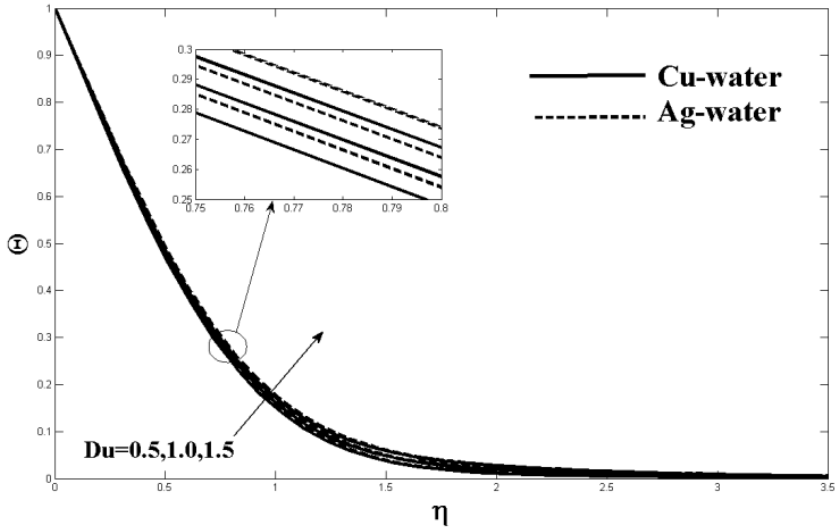

Figure 7. Du on Θ.

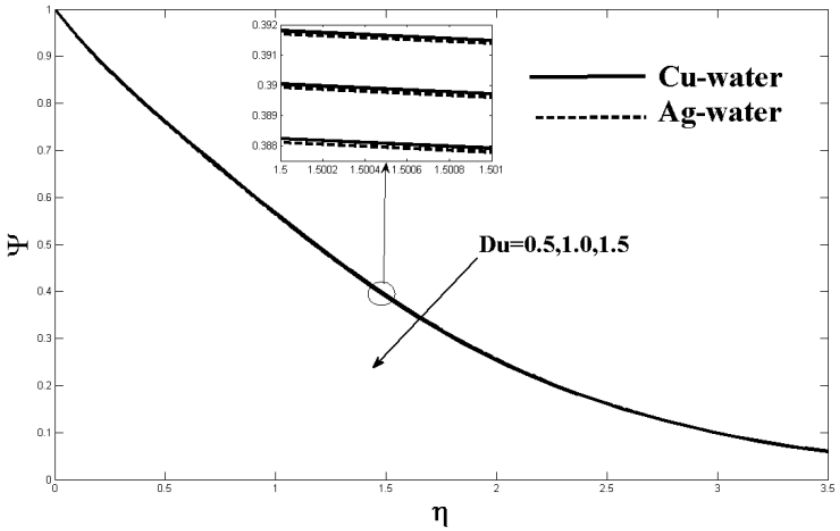

Figure 8. Du on Ψ.

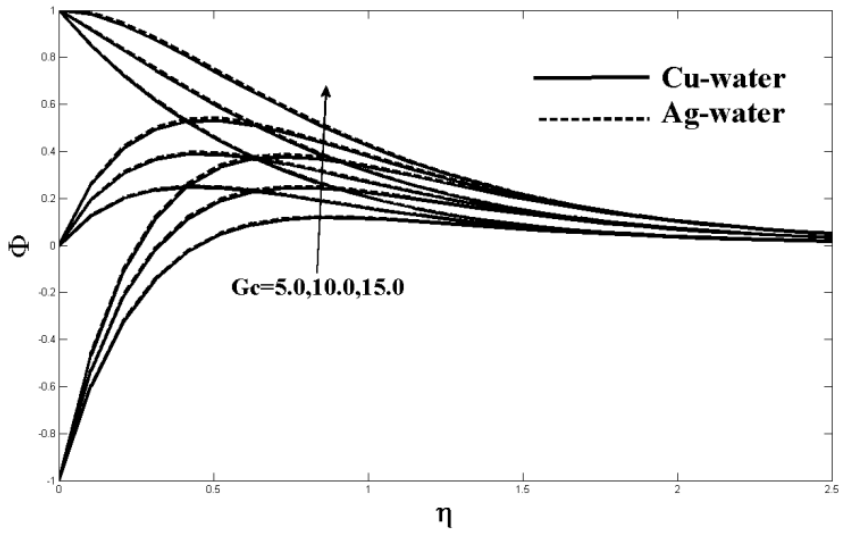

Figure 9. Gc on Φ.

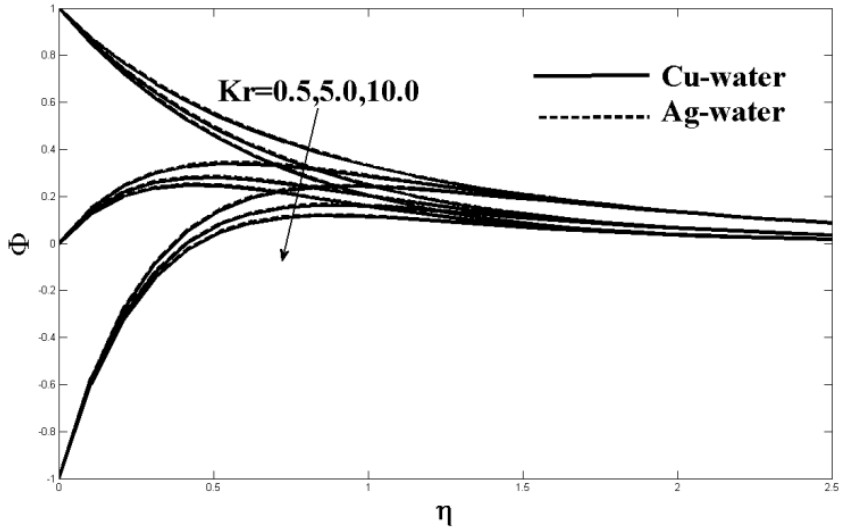

Figure 10. Kr on Φ.

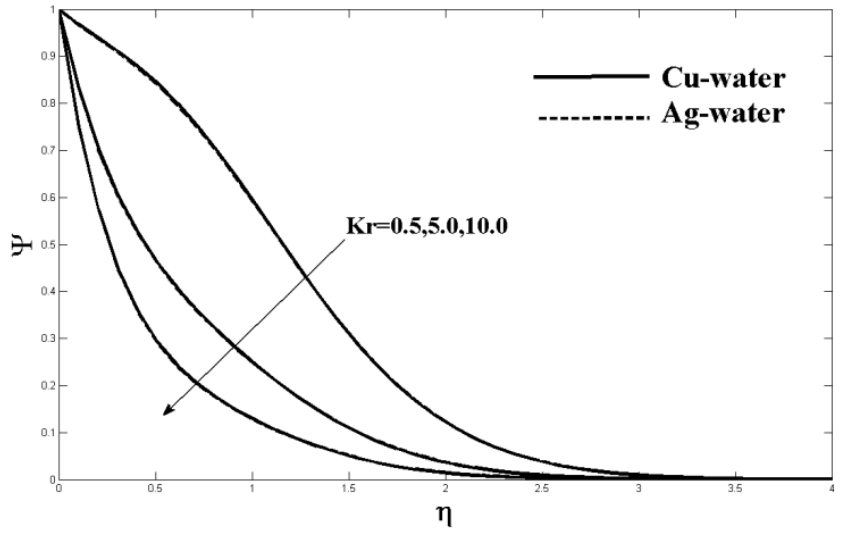

Figure 11. Kr on Ψ.

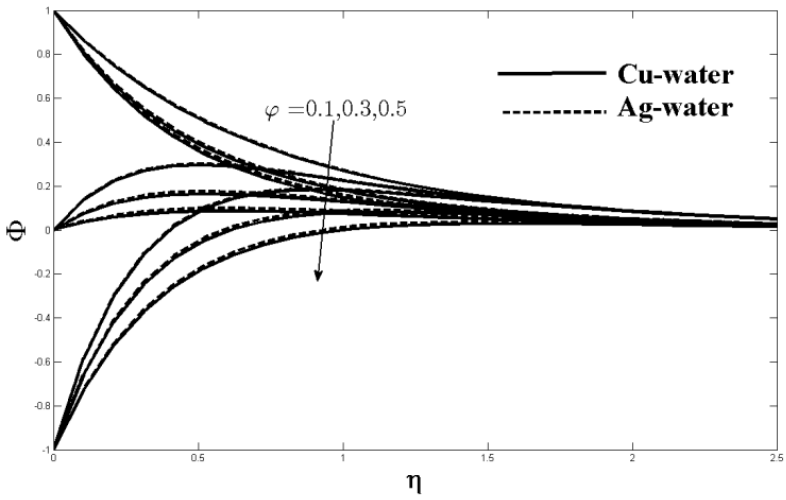

Figure 12. φ on Φ.

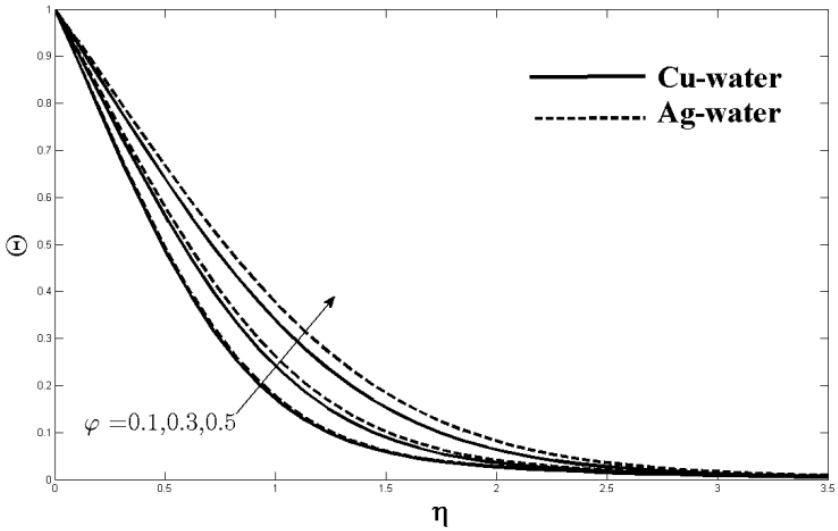

Figure 13. φ on Θ.

Impacts of Sc on Φ and Ψ of both nanofluids are shown in Figures 15 & 16, respectively. With increased Sc values, velocity and species concentration profiles slow down. This is due to a reduction in molecular diffusivity, which causes the concentration and velocity boundary layer thickness to drop. Figures 17 & 18 indicate the impact of *So* on Φ and Ψ of both the nanofluids. Both Φ and Ψ are accelerated with the various values of *So*. Physically, a mass flow is created by the differential in concentration species due to the temperature gradient, as in the case of the Soret effect.

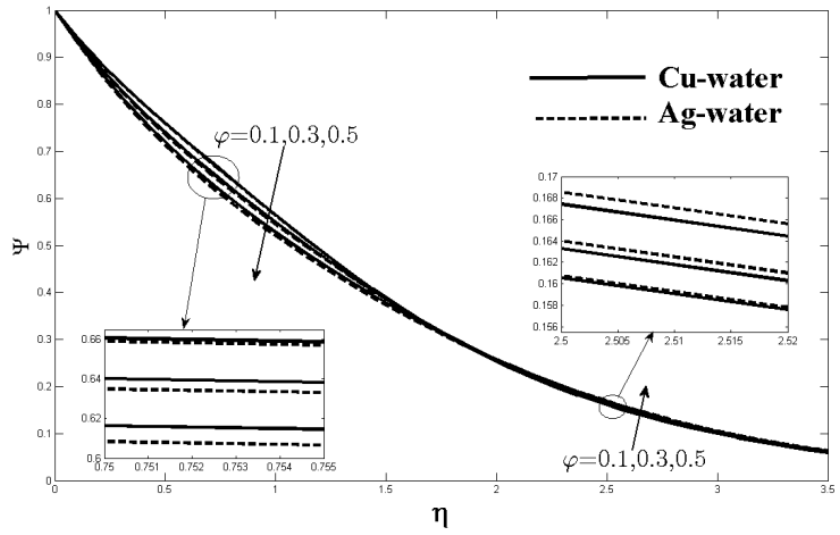

Figure 14. φ on Ψ.

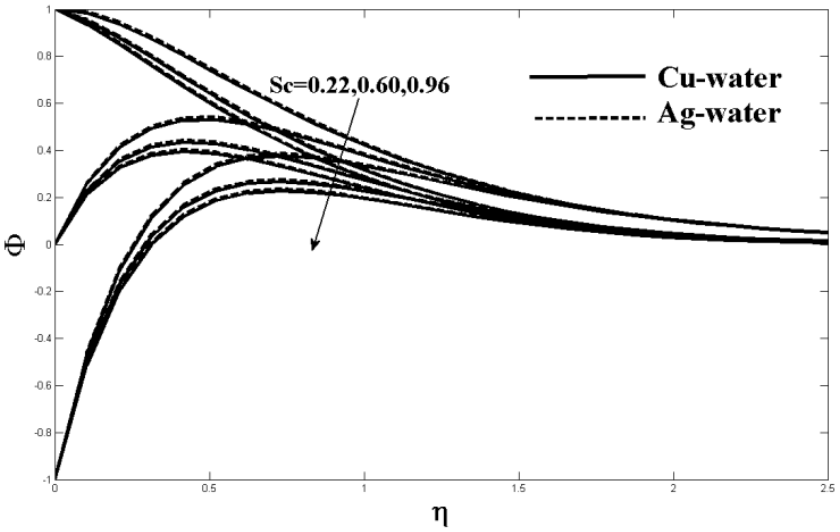

Figure 15. Sc on Φ.

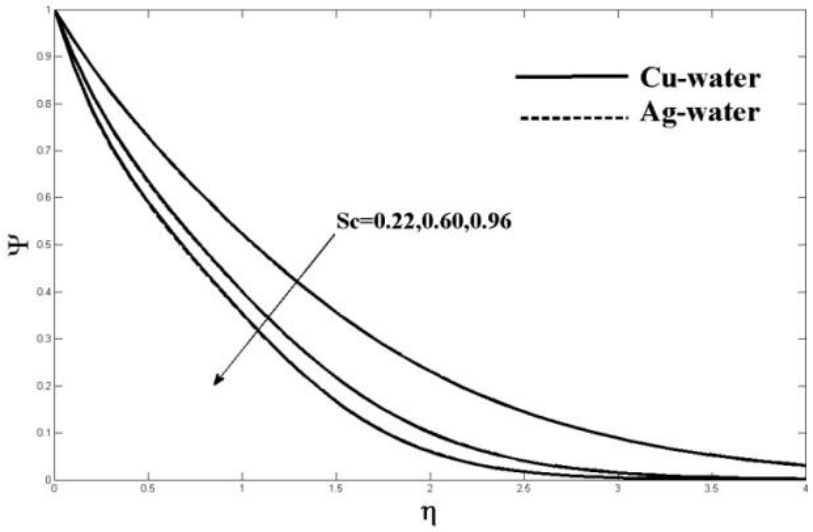

Figure 16. Sc on Ψ.

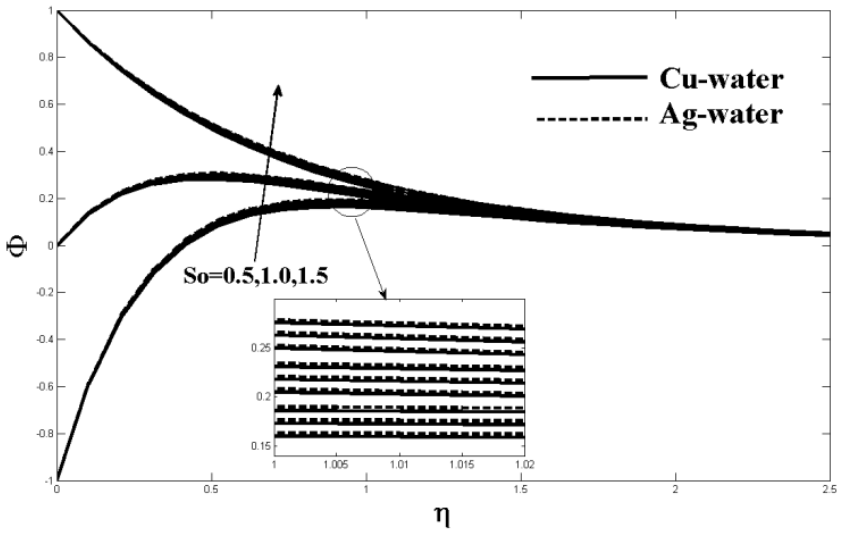

Figure 17. So on Φ.

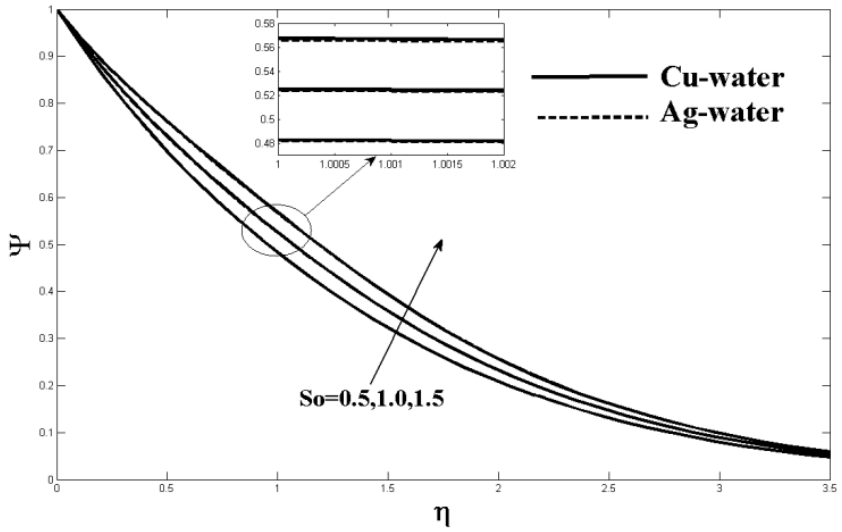

Figure 18. So on Ψ.

Skin friction coefficient τ values of nanoparticles Ag and Cu for stationary and moving plates are presented in Table 2. τ increases the values of *Kr* and diminishes the values of *Nr*, *Q*, *So*, and *Du* for both stationary and moving plates. It can be observed that augmented values of *K* rise in friction coefficient for $\lambda = -1$, whereas decreases for $\lambda = 0,1$. Both *Nu* and *Sh* of nanoparticles Ag and Cu are displayed in Table 3. *Nu* grows for *So* and decreases for *Nr*, *Q*, *Kr*, and *Du* as shown in Table 3, although the Sherwood number differs from the Nusselt number.

Table 2. Skin friction

Nr	Q	So	Kr	K	Du	τ					
						Cu			Ag		
						λ =-1	λ =0	λ =1	λ =-1	λ =0	λ =1
0.5	2	0.6	3	5	0.1	-3.8696	-1.0574	1.7548	-3.8971	-1.0702	1.7566
1.0						-3.8956	-1.0834	1.7288	-3.9232	-1.0963	1.7305
1.5						-3.9165	-1.1043	1.7079	-3.9443	-1.1174	1.7095
	0.5					-3.9165	-1.1043	1.7079	-3.9443	-1.1174	1.7095
	1.0					-3.9177	-1.1055	1.7067	-3.9455	-1.1186	1.7082

Nr	Q	So	Kr	K	Du	τ					
						Cu			Ag		
						λ =-1	λ =0	λ =1	λ =-1	λ =0	λ =1
	1.5					-3.9189	-1.1067	1.7055	-3.9467	-1.1199	1.7070
		0.5				-3.8905	-1.0783	1.7339	-3.9185	-1.0916	1.7353
		1.0				-3.9189	-1.1067	1.7055	-3.9467	-1.1199	1.7070
		1.5				-3.9474	-1.1352	1.6770	-3.9751	-1.1482	1.6786
			0.5			-3.9879	-1.1757	1.6365	-4.0150	-1.1881	1.6387
			5			-3.9194	-1.1072	1.7050	-3.9473	-1.1205	1.7064
			10			-3.8617	-1.0495	1.7627	-3.8902	-1.0634	1.7635
				1		-3.9174	-1.0280	1.8613	-3.9449	-1.0424	1.8601
				2		-3.8828	-1.0413	1.8001	-3.9109	-1.0554	1.8001
				3		-3.8711	-1.0458	1.7794	-3.8995	-1.0598	1.7798
					0.2	-3.8718	-1.0466	1.7787	-3.9002	-1.0606	1.7791
					0.3	-3.8726	-1.0473	1.7779	-3.9010	-1.0613	1.7783
					0.4	-3.8733	-1.0480	1.7772	-3.9017	-1.0621	1.7776

Table 3. Nusselt number and Sherwood number

Nr	Q	So	Kr	K	Du	Nu		Sh	
						Cu	Ag	Cu	Ag
0.5	2	0.6	3	5	0.1	2.3608	2.3323	0.5113	0.5171
1.0						2.0944	2.0689	0.5650	0.5701
1.5						1.9015	1.8783	0.6033	0.6078
	0.5					1.9015	1.8783	0.6033	0.6078
	1.0					1.8804	1.8569	0.6074	0.6121
	1.5					1.8592	1.8353	0.6117	0.6164
		0.5				1.8560	1.8321	0.7475	0.7498
		1.0				1.8592	1.8353	0.6117	0.6164
		1.5				1.8624	1.8385	0.4752	0.4823
			0.5			1.8662	1.8422	0.1880	0.1953
			5			1.8596	1.8356	0.6725	0.6793
			10			1.8532	1.8291	1.0755	1.0819
				1		1.8532	1.8291	1.0755	1.0819
				2		1.8532	1.8291	1.0755	1.0819
				3		1.8532	1.8291	1.0755	1.0819
					0.2	1.8445	1.8202	1.0776	1.0840
					0.3	1.8358	1.8112	1.0796	1.0861
					0.4	1.8271	1.8021	1.0817	1.0883

5. Conclusions

The current study investigates the numerical solution of the Soret, heat source, and Dufour influences on MHD radiating nanofluid flow of Ag-water and Cu-water through a vertical plate inserted in a porous media. The finite-difference approach is used to resolve the resulting equations for momentum, energy, and species concentration. Graphs and tables depict the effects of numerous parameters on fluid attributes like velocity, energy, and species concentration. The following are the main conclusions:

- For the nanoparticles Ag and Cu, the fluid velocity amplifies for increasing values of Du, Gc, and So, diminishing with Kr, φ, and Sc.
- The fluid temperature rises for the nanoparticles Ag and Cu for the augmented Dufour number and volume fraction parameter values.
- For the nanoparticles Ag and Cu, the fluid concentration rises for the larger values of φ and So. In contrast, it reduces the augmented values of the Du, Kr, and Sc.
- Skin frictions decay for the augmented values of Nr, Q, So, K, and Du, whereas it increases by the values of Kr.

- Enlargement of Nr, Q, Kr, and Du enhances the Sherwood number but depreciates the Nusselt number.
- The augmented values of So are depreciating the Sherwood number but enhancing the Nusselt number.

Funding

This research received no external funding.

Acknowledgments

The authors appreciate the anonymous reviewers' insightful comments and recommendations for raising the quality of the paper.

Conflicts of Interest

The authors declare no conflict of interest.

References

1. Choi, S.U.S; Eastman, J.A. Enhancing thermal conductivity of fluids with nanoparticles(No. ANL/MSD/CP-84938; CONF-951135-29). Argonne National Lab.(ANL), Argonne, IL (United States), **1995,** https://www.osti.gov/biblio/196525**.**
2. Veera Krishna, M.; Ameer Ahamad, N.; Chamkha, A. J. Radiation absorption on MHD convective flow of nanofluids through vertically travelling absorbent plate. *Ain Shams Eng. J.* **2021**, *12*, 3043-3056, https://doi.org/10.1016/j.asej.2020.10.028
3. Dharmaiah, G.; Sridhar, W.; Balamurugan, K. S.; Chandra Kala, K. Hall and ion slip impact on magneto-titanium alloy nanoliquid with diffusion thermo and radiation absorption. *International Journal of Ambient Energy*. **2020**, 1-11, doi.org/10.1080/01430750.2020.1831597
4. Khan, N.; Ali, F.; Arif, M.; Ahmad, Z.; Aamina, A.; Khan, I. Maxwell Nanofluid Flow over an Infinite Vertical Plate with Ramped and Isothermal Wall Temperature and Concentration. *Math. Probl. Eng.* **2021**, https://doi.org/10.1155/2021/3536773.
5. Ahmed, K.; Akbar, T.; Muhammad, T.; Alghamdi, M. Heat transfer characteristics of MHD flow of Williamson nanofluid over an exponential permeable stretching curved surface with variable thermal conductivity. *Case Stud. Therm. Eng.* **2021**, *28*, 101544, https://doi.org/10.1016/j.csite.2021.101544.
6. Sravanthi, C. S.; Mabood, F.; Nabi, S. G.; Shehzad, S. A. Heterogeneous and homogeneous reactive flow of magnetite-water nanofluid over a magnetized moving plate. *Propuls. Power Res.* **2022**, *11*, 265-275, https://doi.org/10.1016/j.jppr.2022.02.006.
7. Baby Rani, C. H.; Dharmaiah, G.; Vedavathi, N.; Balamurugan, K. S. Hall and ion slip effects on Ag-water based MHD nanofluid flow over a semi-infinite vertical plate embedded in a porous medium. *Frontiers in Heat and Mass Transfer (FHMT).* **2020**, 14, http://dx.doi.org/10.5098/hmt.14.6
8. Srinivasulu, T.; Goud, B. S. Effect of inclined magnetic field on flow, heat and mass transfer of Williamson nanofluid over a stretching sheet. *Case Stud. Therm. Eng.* **2021**, *23*, 100819, https://doi.org/10.1016/j.csite.2020.100819.
9. Noranuar, W. N. N.; Mohamad, A. Q.; Shafie, S.; Khan, I.; Jiann, L. Y.; Ilias, M. R. Non-coaxial rotation flow of MHD Casson nanofluid carbon nanotubes past a moving disk with porosity effect. *Ain Shams Eng. J.* **2021**, *12*, 4099–4110, https://doi.org/10.1016/j.asej.2021.03.011.
10. Sarkar, A.; Kundu, P. K. Framing the upshot of Hall current on MHD unsteady nanofluid flow from a rotating spherical body in presence of solar radiation. International Journal of Ambient Energy. **2021**, 1-11, doi.org/10.1080/01430750.2021.1965021
11. Swain, K.; Mahanthesh, B. Thermal enhancement of radiating magneto-nanoliquid with nanoparticles aggregation and joule heating: a three-dimensional flow. Arabian Journal for Science and Engineering. **2021**, 46(6), 5865-5873, doi.org/10.1007/s13369-020-04979-5
12. Sharma, R. P.; Prakash, O.; Mishra, S. R.; Rao, P. S. Hall current effect on molybdenum disulfide (MoS2)-engine oil (EO) based MHD nanofluid flow in a moving plate. *International Journal of Ambient Energy*. **2021**, 1-9, doi.org/10.1080/01430750.2021.2003239
13. Veera Krishna, M.; Ameer Ahamad, N.; Aljohani, A. F. Thermal radiation, chemical reaction, Hall and ion slip effects on MHD oscillatory rotating flow of micro-polar liquid. *Alexandria Eng. J.* **2021**, *60*, 3467–3484, https://doi.org/10.1016/j.aej.2021.02.013.
14. Prabhakar Reddy, B.; Sademaki, L. J. A Numerical Study on Newtonian Heating Effect on Heat Absorbing

MHD Casson Flow of Dissipative Fluid past an Oscillating Vertical Porous Plate. *Int. J. Math. Math. Sci.* **2022**, *2022*, 1–16, https://doi.org/10.1155/2022/7987315.
15. Nabwey, H. A.; EL-Kabeir, S. M. M.; Rashad, A. M.; Abdou, M. M. M. Gyrotactic microorganisms mixed convection flow of nanofluid over a vertically surfaced saturated porous media. *Alexandria Eng. J.* **2022**, *61*, 1804–1822, https://doi.org/10.1016/j.aej.2021.06.080.
16. Arulmozhi, S.; Sukkiramathi, K.; Santra, S. S.; Edwan, R.; Fernandez-Gamiz, U.; Noeiaghdam, S. Heat and mass transfer analysis of radiative and chemical reactive effects on MHD nanofluid over an infinite moving vertical plate. *Results Eng.* **2022**, *14*, 100394, https://doi.org/10.1016/j.rineng.2022.100394.
17. Rooman, M.; Jan, M. A.; Shah, Z.; Kumam, P.; Alshehri, A. Entropy optimization and heat transfer analysis in MHD Williamson nanofluid flow over a vertical Riga plate with nonlinear thermal radiation. *Sci. Rep.* **2021**, *11*, 1–14, https://doi.org/10.1038/s41598-021-97874-4.
18. Krishna, M. V.; Ahammad, N. A.; Chamkha, A. J. Radiative MHD flow of Casson hybrid nanofluid over an infinite exponentially accelerated vertical porous surface. *Case Stud. Therm. Eng.* **2021**, *27*, 101229, https://doi.org/10.1016/j.csite.2021.101229.
19. Wahid, N. S.; Md Arifin, N.; Khashi'ie, N. S.; Pop, I.; Bachok, N.; Hafidzuddin, M. E. H. MHD mixed convection flow of a hybrid nanofluid past a permeable vertical flat plate with thermal radiation effect. *Alexandria Eng. J.* **2022**, *61*, 3323–3333, https://doi.org/10.1016/j.aej.2021.08.059.
20. Kumar, M. A.; Reddy, Y. D.; Rao, V. S.; Goud, B. S. Thermal radiation impact on MHD heat transfer natural convective nano fluid flow over an impulsively started vertical plate. *Case Stud. Therm. Eng.* **2021**, *24*, 100826, https://doi.org/10.1016/j.csite.2020.100826.
21. Ullah, H.; Khan, M. A.; Fiza, M.; Ullah, K.; Ayaz, M.; Al-Mekhlafi, S. M. Analytical and Numerical Analysis of the Squeezed Unsteady MHD Nanofluid Flow in the Presence of Thermal Radiation. Journal of Nanomaterials. **2022**, doi.org/10.1155/2022/1668206
22. Rahman, M.; Uddin, J. Magnetohydrodynamic boundary layer flow of nanofluid with variable chemical reaction in a radiative vertical plate. Heat Transf. **2021**, vol. 50, no. 8, pp. 7879–7897, doi: 10.1002/htj.22258
23. Goud Bejawada, S.; Dharmendar Reddy, Y.; Jamshed, W.; Nisar, K. S.; Alharbi, A. N.; Chouikh, R. Radiation effect on MHD Casson fluid flow over an inclined nonlinear surface with chemical reaction in a Forchheimer porous medium: Radiation effect on MHD Casson fluid flow over an inclined nonlinear surface. *Alexandria Eng. J.* **2022**, *61*, 8207–8220, https://doi.org/10.1016/j.aej.2022.01.043.
24. Patil, A. B.; Humane, P. P.; Patil, V. S.; Rajput, G. R. MHD Prandtl nanofluid flow due to convectively heated stretching sheet below the control of chemical reaction with thermal radiation. International Journal of Ambient Energy. **2021**, 1-13, doi.org/10.1080/01430750.2021.1888803
25. Cui, J.; Munir, S.; Raies, S. F.; Farooq, U.; Razzaq, R. Non-similar aspects of heat generation in bioconvection from flat surface subjected to chemically reactive stagnation point flow of Oldroyd-B fluid. *Alexandria Eng. J.* **2022**, *61*, 5397–5411, https://doi.org/10.1016/j.aej.2021.10.056.
26. Mondal, H.; Pal, D.; Chatterjee, S.; Sibanda, P. Thermophoresis and Soret-Dufour on MHD mixed convection mass transfer over an inclined plate with non-uniform heat source/sink and chemical reaction. *Ain Shams Engineering Journal* **2018**, *9*, 2111-2121, https://doi.org/10.1016/j.asej.2016.10.015.
27. Oyekunle, T. L.; Agunbiade, S. A. Diffusion-thermo and thermal-diffusion effects with inclined magnetic field on unsteady MHD slip flow over a permeable vertical plate. *J. Egypt. Math. Soc.* **2020**, *28*, https://doi.org/10.1186/s42787-020-00110-7.
28. Ahammad, N. A.; Krishna, M. V. Numerical investigation of chemical reaction, Soret and Dufour impacts on MHD free convective gyrating flow through a vertical porous channel. *Case Stud. Therm. Eng.* **2021**, *28*, 101571, https://doi.org/10.1016/j.csite.2021.101571.
29. Siddique, I.; Nadeem, M.; Awrejcewicz, J.; Pawłowski, W. Soret and Dufour effects on unsteady MHD second-grade nanofluid flow across an exponentially stretching surface. Scientific Reports. **2022**, 12(1), 1-14, doi.org/10.1038/s41598-022-16173-8
30. Ganga, B.; Mohamed Yusuff Ansari, S.; Vishnu Ganesh, N.; Abdul Hakeem, A. K. MHD flow of Boungiorno model nanofluid over a vertical plate with internal heat generation/absorption. *Propuls. Power Res.* **2016**, *5*, 211–222, https://doi.org/10.1016/j.jppr.2016.07.003.
31. Anwar, T.; Kumam, P.; Shah, Z.; Watthayu, W.; Thounthong, P. Unsteady radiative natural convective MHD nanofluid flow past a porous moving vertical plate with heat source/sink. *Molecules* **2020**, *25*, 1–21, https://doi.org/10.3390/molecules25040854.
32. Dharmaiah, G.; Makinde, O. D.; Balamurugan, K. S. Perturbation analysis of thermophoresis, hall current and heat source on flow dissipative aligned convective flow about an inclined plate. Int. J. Thermofluid Sci. Tech. **2020**, 7(1), doi.org/10.36963/IJTST.20070103
33. Mishra, A.; Pandey, A. K.; Chamkha, A. J.; Kumar, M. Roles of nanoparticles and heat generation/absorption on MHD flow of Ag–H2O nanofluid via porous stretching/shrinking convergent/divergent channel. Journal of the Egyptian Mathematical Society. **2020**, 28(1), 1-18, doi.org/10.1186/s42787-020-00079-3.
34. Patel, H. R. Cross diffusion and heat generation effects on mixed convection stagnation point MHD Carreau fluid flow in a porous medium. *Int. J. Ambient Energy* **2021**, https://doi.org/10.1080/01430750.2021.1931960.
35. Mishra, A.; Pandey, A. K.; Kumar, M. Velocity, thermal and concentration slip effects on MHD silver-water

nanofluid flow past a permeable cone with suction/injection and viscous-ohmic dissipation. *Heat Transf. Res.* **2019**, *50*, 1351–1367, https://doi.org/10.1615/HeatTransRes.2018020420.
36. Chandra Reddy, P.; Raju, M. C.; Raju, G. S. S.; Varma, S. V. K. Free convective magneto-nanofluid flow past a moving vertical plate in the presence of radiation and thermal diffusion. *Front. Heat Mass Transf.* **2016**, *7*, https://doi.org/10.5098/HMT.7.28.
37. Tlili, I.; Samrat, S. P.; Sandeep, N.; Nabwey, H. A. Effect of nanoparticle shape on unsteady liquid film flow of MHD Oldroyd-B ferrofluid. Ain Shams Engineering Journal. **2021**, 12(1), 935-941, doi.org/10.1016/j.asej.2020.06.007
38. Kakaç, S.; Pramuanjaroenkij, A. Review of convective heat transfer enhancement with nanofluids. *Int. J. Heat Mass Transf.* **2009**, *52*, 3187–3196, https://doi.org/10.1016/j.ijheatmasstransfer.2009.02.006.